Pergamon

*Journal of Structural Geology*, Vol. 18, No. 6, pp. 719 to 733, 1996

0191-8141/96 $15.00 + 0.00

0191-8141(95)00140-9

# High-temperature microstructures and rheology of deformed granite, Erzgebirge, Bohemian Massif

KAREL SCHULMANN

Univerzita Karlova, Praha, Czech Republic

BEDŘICH MLČOCH

Czech Geological Survey, Praha, Czech Republic

and

RADEK MELKA*

Univerzita Karlova, Praha, Czech Republic

(*Received* 15 *August* 1994; *accepted in revised form* 29 *November* 1995)

**Abstract**—Three stages of granite deformation were recognized in porphyric granitoids sheared under amphibolite facies conditions in the Erzgebirge Mts: (1) weakly deformed granite in lozenge-shaped pods, (2) S–C orthogneiss, and (3) thin zones of banded mylonites.

Weakly deformed granite forms a load-bearing framework (LBF) structure in which quartz and feldspar aggregates exhibit similar strain intensities and shapes. K-feldspar deforms by fracturing and onset of dynamic recrystallization along clast margins, plagioclase recrystallizes completely and quartz shows effects of grain boundary migration recrystallization and activity of basal ⟨a⟩ slip. S–C orthogneiss is interpreted as an interconnected weak layer (IWL) structure with high viscosity contrast between quartz and both feldspars. Concentration of deformation into thin quartz layers is indicated by intense strain of quartz, grain size variations of recrystallized quartz and dominant prism ⟨a⟩ slip. Feldspars show well annealed structures and slip on (010)⟨001⟩. Banded mylonite is marked by similar strain intensity of quartz and feldspar aggregates and low viscosity contrast between constituent phases. Quartz shows evidence for grain size increase and rhomb ⟨a + c⟩ slip. Fully recrystallized feldspars show evidence for (010)⟨100⟩ slip.

The whole microstructural sequence and the transitions from LBF structure to IWL structures show the dependence of microstructural evolution of different materials on the bulk strain intensity. Copyright © 1996 Elsevier Science Ltd

## INTRODUCTION

Because of the widespread occurrence of granitoids in the crust, the evolution of mylonitic fabrics during granite deformation has been the goal of many studies in the last two decades (e.g. Bossiére & Vauchez 1978, Burg & Laurent 1978, Simpson 1985, Vauchez 1987, Gapais 1989a).

Gapais (1989b) has shown that the strain localization in granitoids is strongly dependent on thermal conditions of deformation and deformation intensity. According to his concept, deformation is extremely heterogeneous at low temperatures and/or low strains, in which case arrays of discrete shear zones enveloping lozenge-shaped, low-strain domains develop. Localized deformation is a transient feature and, with increasing strain, a pervasive S–C fabric and even a homogeneous steady state microstructure are formed at all scales. At higher temperature the deformation is less heterogeneous from the early stages of rock deformation onwards, and the pervasive S–C fabric and steady state microstructures develop at low strain.

The deformation behaviour of granitoids is governed by the contrasting rheologies of constituent minerals, their relative abundance and structure (Gapais 1989a, Handy 1990). Two types of end-member structure can occur (Handy 1990): (1) a load-bearing framework (LBF) in which stronger phases form a skeleton containing isolated weaker domains, and (2) interconnected weak layers (IWL), where a weak matrix encloses boudins of clasts of stronger material. Changes in the internal structure of deformed granite are governed by the microstructural evolution of different minerals. The microstructures and deformation mechanisms of constitutive minerals are temperature dependent and progressively change either with changing temperature (Knipe 1989) or with increasing deformation intensity (Gapais 1989b). These changes lead to a progressive evolution of the local structure, a decrease of bulk rock strength (Jordan 1987, 1988) and to a change in the rheological behaviour of the rock.

The aim of this paper is to describe the deformation and associated microstructural development of a gra-

*Deceased.

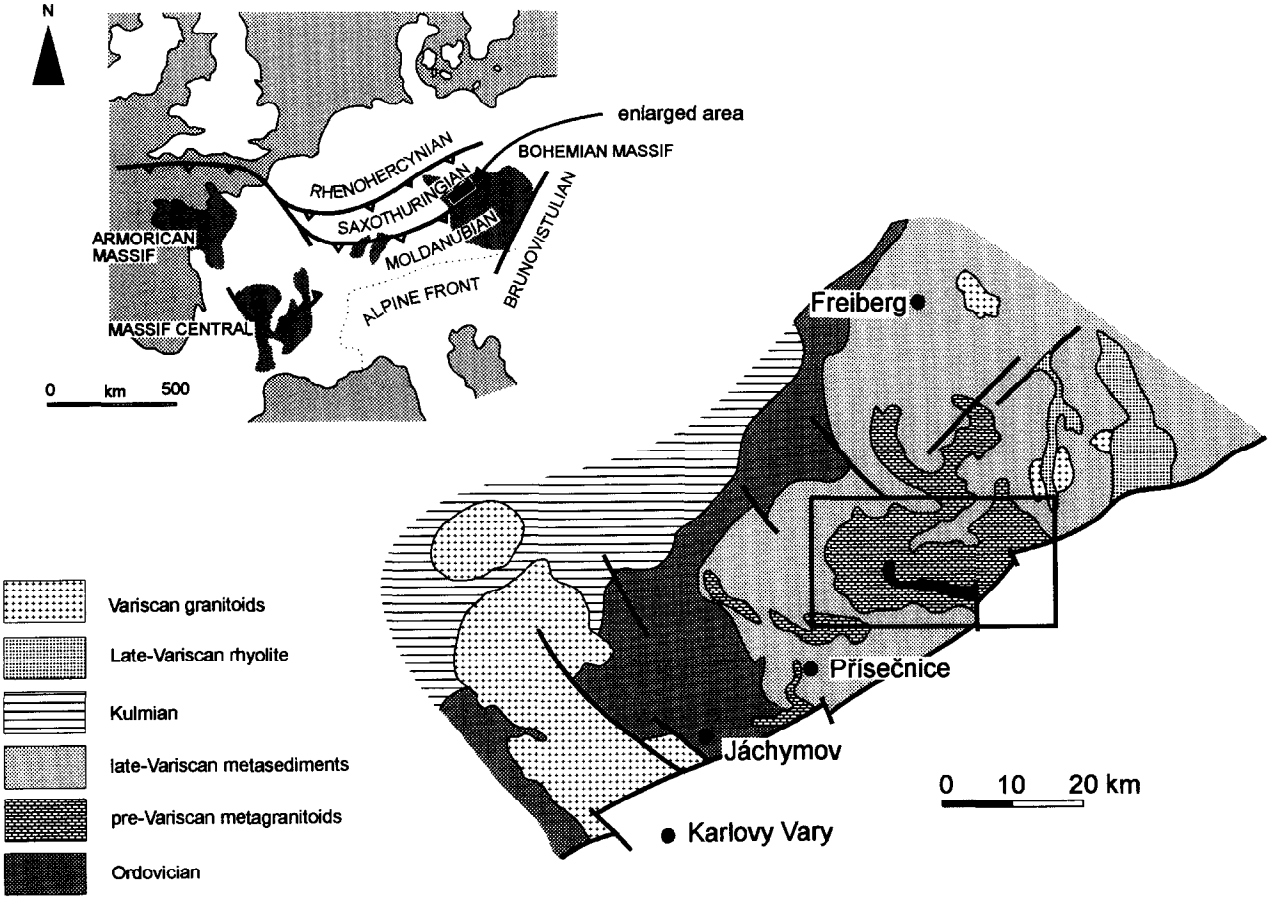


Fig. 1. Geological map of the Erzgebirge crystalline. Upper-left inset shows position of the Erzgebirge crystalline complex within the framework of the European Variscides.

nite, from weakly deformed through S–C granite to banded mylonite. Changes in microstructures and microfabrics in rheologically contrasting minerals are used to document changes in stress, strain and strain rate partitioning in a non-ideal natural polyphase system.

## GEOLOGICAL SETTING

A porphyric, coarse-grained granite, known as 'rote Gneiss' by Scheumann (1932), cropping out in the central part of the Erzgebirge mountains, western Bohemian massif, was chosen for this study. This granitoid is dated at 553 ± 9 – 554 ± 7 Ma using zircon evaporization method (Kröner *et al.* 1995), and it intruded Upper-Proterozoic metasediments of the Saxothuringian basement of the Variscan belt (Fig. 1). This pre-Variscan coarse-grained porphyritic granite forms the core of a large-scale antiformal structure mantled by anatectic banded orthogneiss and paragneiss (Fig. 2). Mlcoch and Schulmann (1991) have suggested pre-Variscan gneiss doming in the central part of Erzgebirge as a mechanism for steepening of migmatitic fabrics around the granitic core.

The granite in the core of antiform and the surrounding migmatitic orthogneiss and paragneiss were strongly deformed during Variscan ductile shearing. The deformation is heterogeneous producing: (1) pervasive S–C granite as the most abundant rock type forming about 90% of outcrops (Fig. 2); (2) low-strain domains that elongate in an E–W direction, and are tens to hundreds of meters in width; (3) scarce high-strain zones of banded mylonites up to 1 m in width.

Kröner *et al.* (1995) estimated local temperatures and pressures around 600°C and 8 kbar for the main Variscan tectonometamorphic event. Later extension occurred under slightly lower temperature corresponding to 550°C and significantly lower pressure 4 kbar (Kröner *et al.* 1995). The pressure estimates are based essentially on phengite barometry and are related to white micas in deformed orthogneiss while the temperatures were inferred from temperature sensitive equilibria in metabasite inclusions within the granite.

The flat-lying Variscan mylonitic foliation bear an E–W trending stretching lineation marked by the elongation of quartz–feldspar aggregates and biotite clusters. Ubiquitous S–C relationships, shear bands and asymmetrical porphyroclast systems indicate top-to-the-west sense of shear. Transitions from low-strain domains to banded mylonites yield suitable examples for the study of the microfabric evolution and for assessment of rheological behaviour of granites under amphibolite facies conditions.

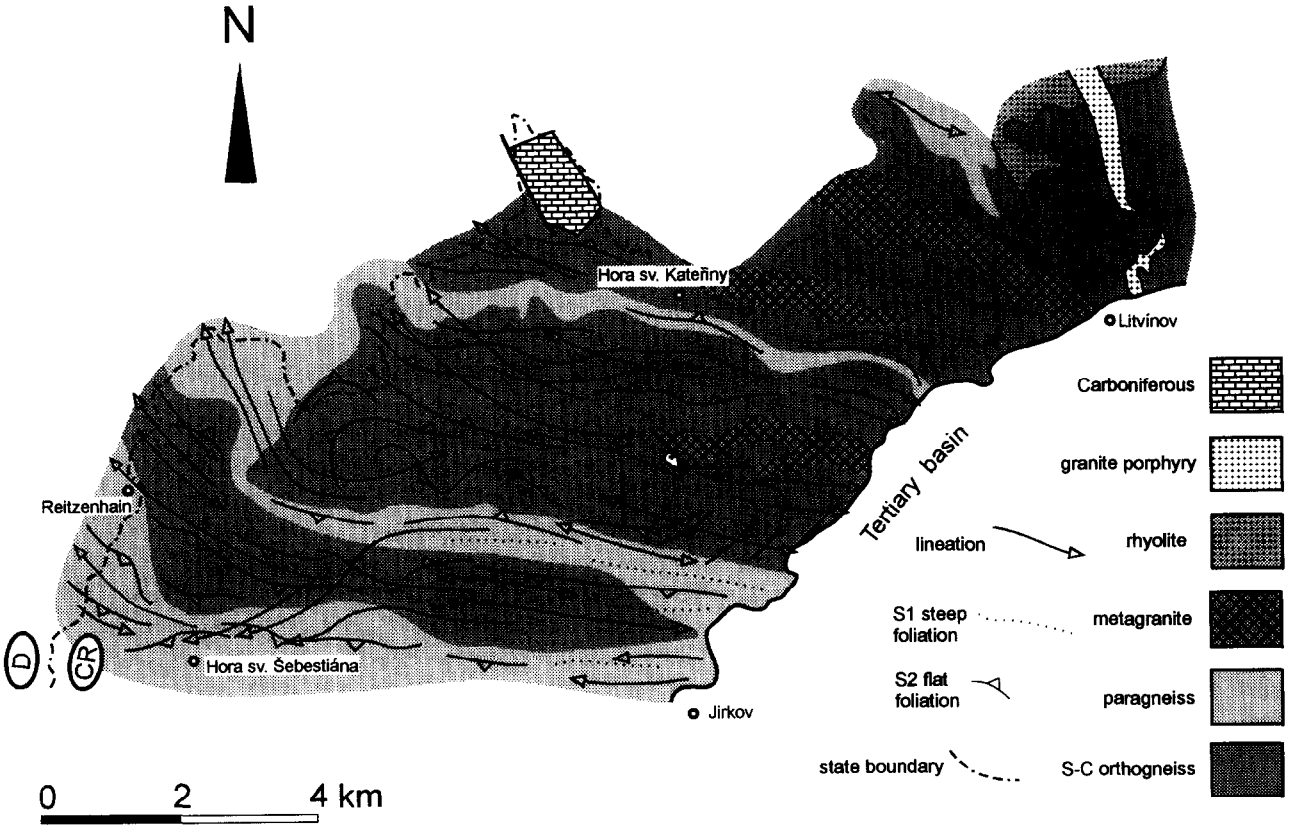


Fig. 2. Structural map of the Catherine dome in the central Erzgebirge. Dip of $S_2$ flat foliation does not exceed 20°. The dip of the early $S_1$ foliation varies between 60° and 80°.

## MICROSTRUCTURAL DEVELOPMENT OF DEFORMED GRANITE

### *Stage I—weakly deformed granite*

Rocks within low-strain areas show only rarely well-preserved primary granitic microstructures (Fig. 3a). The original granite consists of K-feldspar (30–35%), often present as perthitic carlsbad twinned phenocrysts 2–3 cm in size, oligoclase (20%), quartz (35%), biotite (8%) and muscovite (6%). A weak magmatic shape preferred orientation of felsic minerals is present.

More often the granite in low-strain domains shows signs of plastic deformation. Tabular K-feldspar phenocrysts (2–3 cm in size) are fractured, recrystallized at their grain margins and are cut by microshear zones where new grains (100–150 $\mu$m in size) have developed (Fig. 4a). The grains are sub-equant or slightly elongate with straight boundaries and are rectangular in shape. Undulatory extinction of K-feldspar is common.

Plagioclase recrystallization is more pronounced than that of K-feldspar and in some places original large grains are completely converted to a recrystallized matrix (Fig. 4a). Rare plagioclase clasts contain large equigranular subgrains, 100–200 $\mu$m in size with straight boundaries, parallel to the (010) or (001) planes or diagonal to them. Commonly, the subgrains laterally pass to dynamically recrystallized grains of the same size forming an equigranular mosaic (White 1975b). A typical feature is the local growth of idiomorphic flakes of muscovite (0.15–0.3 mm in size) along crystallographic (010) and (001) planes of feldspars.

Quartz forms large grains (1–1.5 cm in size) that have recrystallized mainly at contacts with feldspars, forming new grains with variable shape and size (0.05–1 mm). Irregular boundaries of the new grains (Fig. 4b) indicate grain boundary migration (Poirier & Guillopé 1978). Idiomorphic large micas are kinked and exhibit undulatory extinction and dynamic recrystallization at their margins.

With increasing strain, the grain sizes of recrystallized grains are not uniformly distributed and vary between 400 and 700 $\mu$m (Fig. 5). The recrystallized grain size of quartz is significantly larger than that of plagioclase and K-feldspar (Figs. 4b and 5). Quartz and micas show comparatively greater amounts of fine-grained fraction due to recrystallization while the large spread of feldspar grain size is due to relics of clasts. Average grain size versus standard deviation exhibits an approximately linear relationship (Fig. 5).

Model analyses have shown that the undeformed granite consists of about 60–65% feldspar (Fig. 6) and 35–40% quartz and micas. We consider K-feldspar as the rheologically 'strongest' phase, plagioclase is relatively weaker and quartz and micas represent the 'weakest' phases. The line-transect method has been used to determine the number of mutual contacts between individual grains, to assess the degree of contiguity of individual phases (Mitra 1978). Grain contact analyses show that 10–15% of contacts are 'hard' (i.e. contacts

between feldspars), 60–75% are 'weak' (between weak minerals) and 10–30% are 'hard–weak' contacts. These textural relations reflect the significantly larger grain size of hard grains with respect to small weak grains.

Large amounts of a stronger phase composed of large particles (60%) together with a small number of mutual 'hard contacts' (10%) are indicative of a sponge-like configuration of the stronger fraction that forms an original rigid skeleton. The weak fraction, comprising smaller recrystallized minerals, fills the space within the feldspar framework. This configuration, characteristic for exceptionally weakly deformed granite, is comparable to Handy's (1990) LBF structure.

*Stage II—S–C orthogneiss*

Typical augen orthogneiss with well defined S–C structure (Berthé *et al.* 1979) developed as a result of non-coaxial deformation of the porphyric granite (Fig. 3b & c).

K-feldspar porphyroclasts are often rotated and lie with their largest (010) crystal face subparallel to the foliation plane (Debat *et al.* 1978). K-feldspar is strongly recrystallized resulting in two types of recrystallized microstructures (Hanmer 1982):

(1) Relatively wide zones of new equigranular grains (50 $\mu$m to 150 $\mu$m in diameter) develop at the margins of porphyroclasts, forming a core-mantle structure (White 1975a). The mantles are made of new K-feldspar grains, very small sodic plagioclase and small quartz drops at the contacts of new K-feldspar grains.

(2) New discrete recrystallized grains develop from subgrains in the inner parts of perthitic K-feldspar clasts. Subgrains in the core of relict clasts are elongate, rectangular in shape, 100–150 $\mu$m in size and limited by string perthite walls mostly parallel to (010) planes. Continued deformation leads to the formation of new rectangular K-feldspar grains with optically sharp, straight boundaries only rarely meeting in triple point junctions (Fig. 7). In recrystallized tails new grains at K-feldspar are subequant in shape and meet more commonly in triple point junctions (Fig. 7).

Myrmekites develop at foliation-parallel sides of the K-feldspar augens (Simpson & Wintsch 1989, Vernon 1991). Locally, they may totally replace the original grain. Aggregates of fine-grained dynamically recrystallized plagioclase and quartz grains develop behind the myrmekitic front.

Plagioclase is commonly fully recrystallized forming sub-equant new grains with straight boundaries. Ideal 120° triple points are most common (Fig. 7). The new grains are optically strain-free and show continuous twins. Small interstitial white micas commonly grow along margins of individual grains.

Quartz is present in aggregates of slightly elongate (aspect ratio, 2:1) or subequant grains with serrated boundaries (Fig. 4c). The size of these new grains is commonly 80 to 300 $\mu$m. Quartz aggregates are commonly wrapped around large feldspar porphyroclasts, where the size of quartz grains is strongly reduced. Subequant $\mu$m-size quartz grains occur in narrow areas pinched between feldspar clasts. In areas where the spacing of feldspar clasts is greater, the new grains are larger (50–80 $\mu$m in size), elongate, and form a characteristic shape with preferred orientation oblique to the foliation. The variations in grain size reflect stress gradients within the quartz phase. The angle of obliquity of recrystallized quartz aggregates varies on the scale of a thin-section.

Biotite and muscovite form elongate, band-like aggregates which are clearly separated from each other.

The analysis of grain size distribution of individual mineral phases reveals an abrupt decrease of grain size due to an increase in the recrystallized fraction of all mineral phases. The decrease in the average grain size of quartz and both feldspars is accompanied by decrease of the standard deviation (Fig. 5). The size of muscovite and biotite is uniform. Grain contact analysis reveals an increase of aggregate distribution of all felsic minerals (Fig. 6) due to their extensive recrystallization.

Modal analysis (Fig. 6) shows that the augen orthogneiss consists of approximately 55% feldspars and 45% quartz and micas indicating a slight increase in the amount of the weak, quartz–mica fraction. Considerable increase of hard–hard contacts with respect to the weakly deformed granite is due to mechanical segregation of weak and strong layers to form contiguous aggregates oriented subparallel to the plane of shear (Knipe & Wintsch 1985). Simultaneous decrease of the amount of weak contacts results from selected shrinkage and growth of adjacent quartz grains, leading towards a more unified grain size and to a decrease in the number of grains (Jessell 1986). The original granitic sponge-like configuration of the hard fraction is destroyed in the course of intense recrystallization of feldspars and concentration of the recrystallized material into tails oriented subparallel to the shear plane. This stage of granite deformation corresponds to IWL structure with a low volume proportion of the weak fraction (quartz and micas) and high viscous strength contrast between the recrystallized matrix and relic feldspar clasts.

*Stage III—banded quartz–feldspar mylonite*

Banded quartz–feldspar mylonite is the final product of granite deformation (Fig. 3d) marked by complete recrystallization of all minerals. K-feldspar layers are formed by recrystallized and slightly elongate grains. Ribbon cores show curved grain boundaries. Ribbon mantles are made of a fine-grained mixture of plagioclase, K-feldspar and quartz. This structure results from the deformation of myrmekite rims which originally surrounded the large K-feldspar porphyroclasts.

Plagioclase aggregates comprise an equigranular mosaic of elongate recrystallized grains of the same grain size as those of K-feldspar new grains (Figs. 4d and 5). Quartz forms polycrystalline ribbons, one grain wide, composed of elongate, rectangular grains 150–250 $\mu$m in size. Grains have straight boundaries commonly perpendicular to ribbon margins (Fig. 4d). Typical inter-

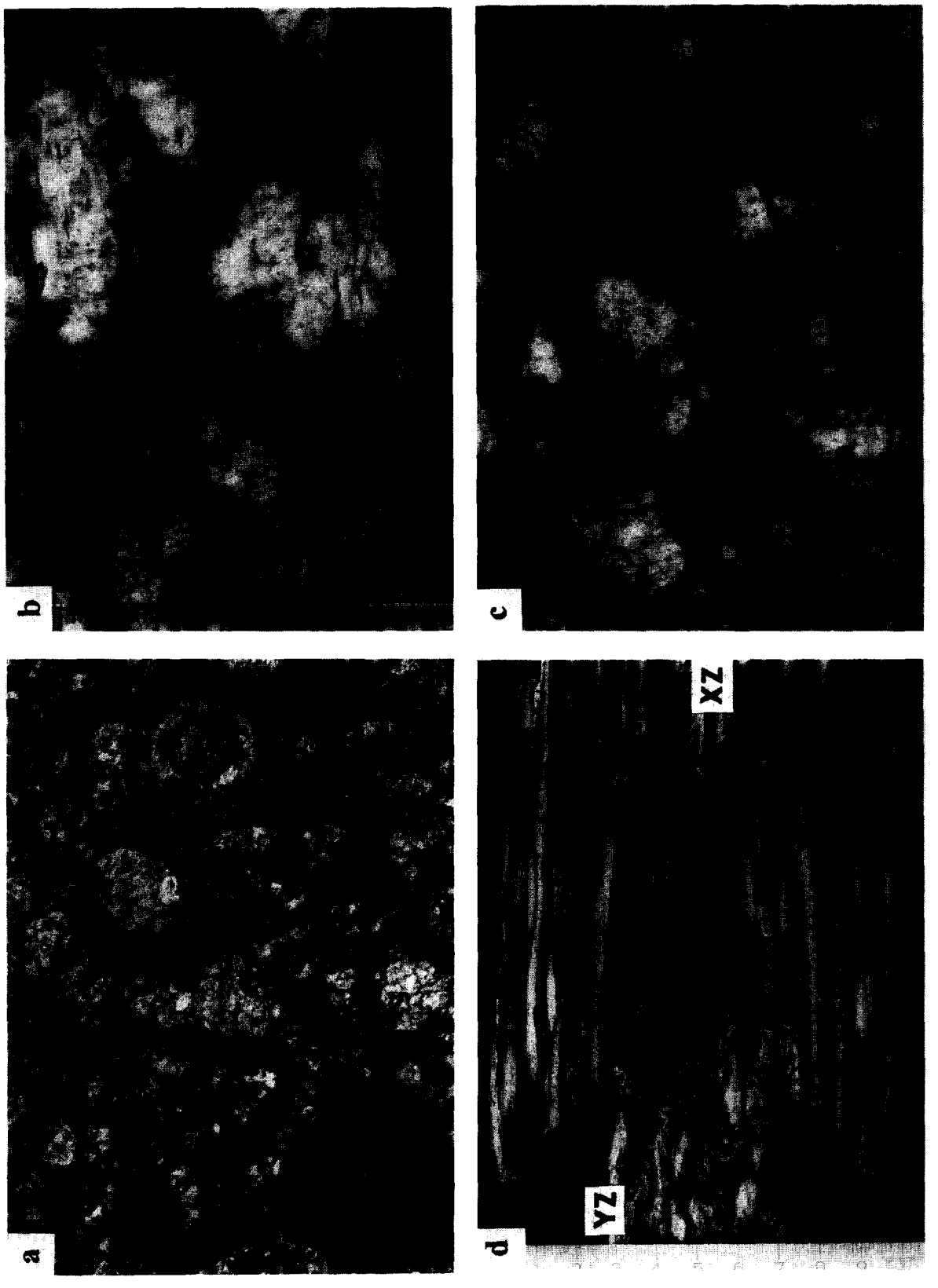


Fig. 3. Three stages of progressive deformation of the Erzgebirge granite. (a) Undeformed metagranite (stage I), (b) and (c) S–C orthogneiss (stage II), XZ and YZ sections respectively. (d) banded mylonite (stage III), XZ and YZ sections.

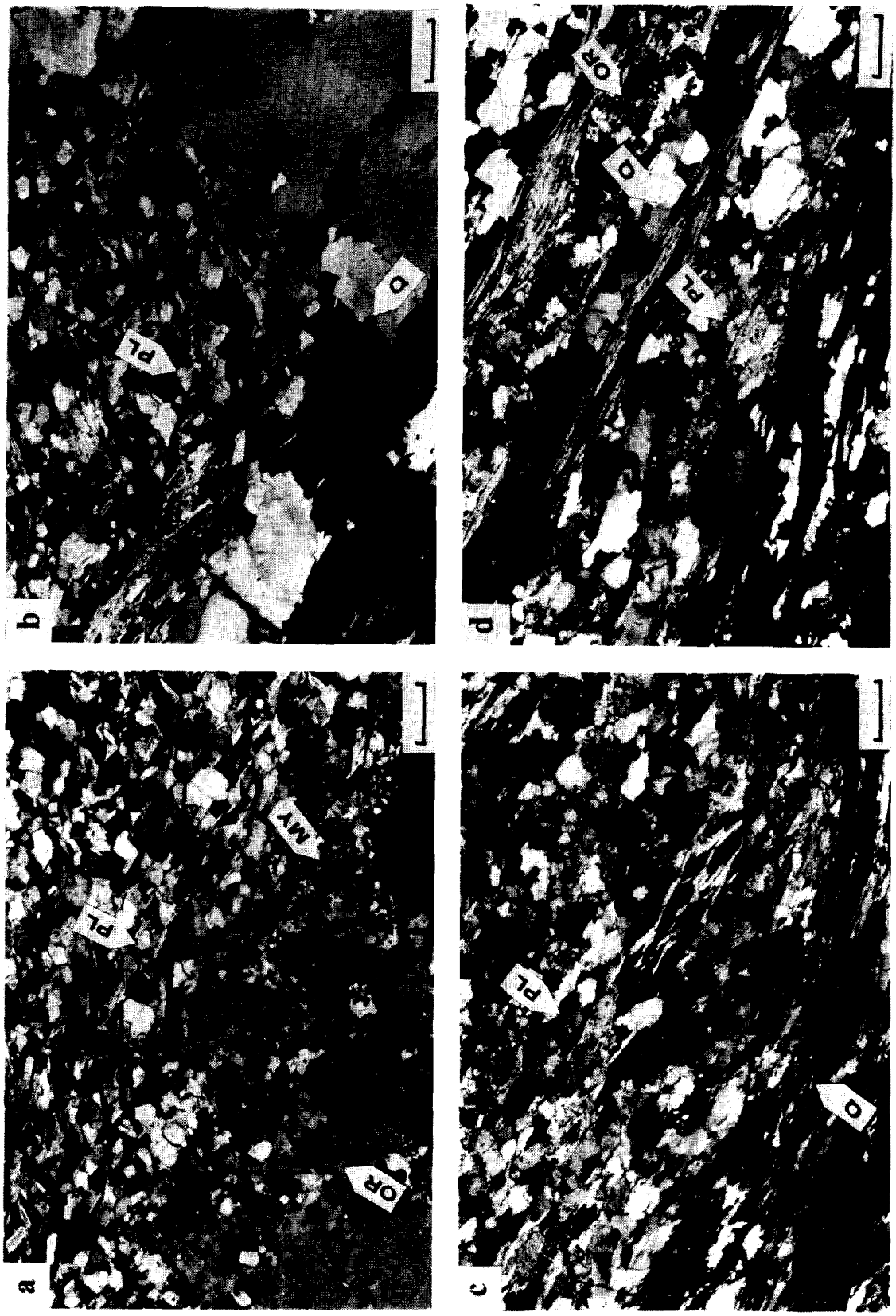


Fig. 4. (a) Contact between a K-feldspar grain and a recrystallized plagioclase mosaic in weakly deformed granite. Note incipient recrystallization of K-feldspar along microshear zones, whereas plagioclase is totally converted to a recrystallized foam texture. (b) Contact between recrystallized plagioclase and recrystallized quartz in weakly deformed granite. Grain size of recrystallized quartz significantly exceeds that of plagioclase and exhibits no reduction related to plagioclase boundaries. (c) Contact between recrystallized plagioclase foam texture and recrystallized quartz in S–C orthogneiss. Significant variations in quartz grain size reflects variations in stress distribution. (d) Banded structure of mylonite shows large equilibrated quartz grains in contact with recrystallized plagioclase and K-feldspar layers. Lack of variations in grain size indicates uniformly distributed stress in the rock. Scale bar, 0.5 mm.

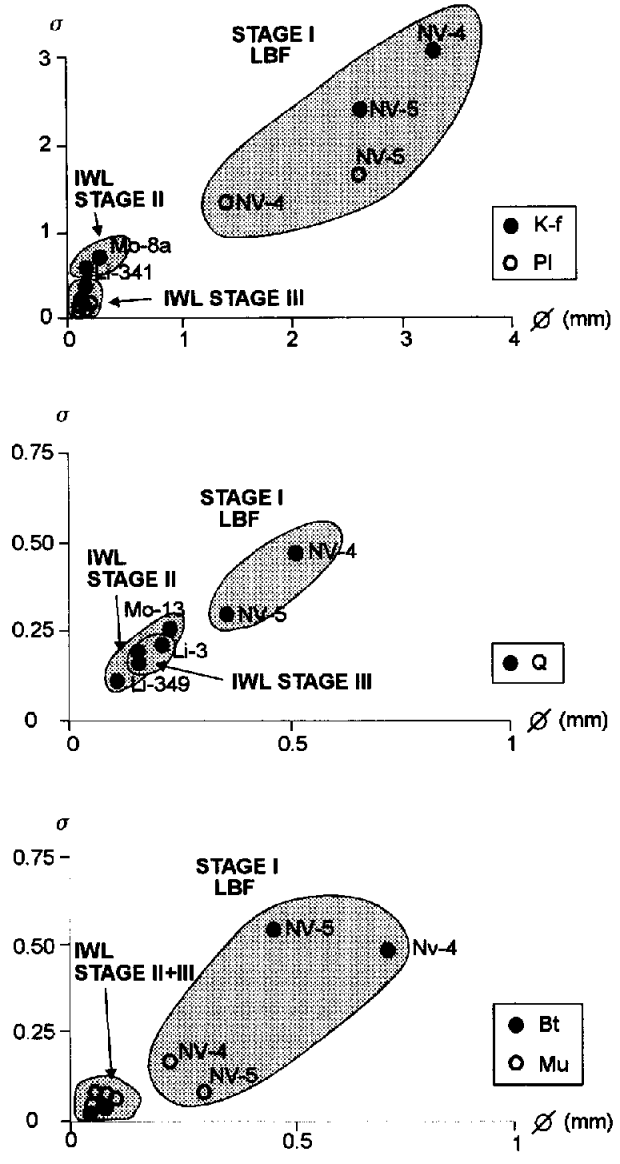


Fig. 5. Orthogonal plots of average grain size versus grain size standard deviation of K-feldspar (Kf), plagioclase (Pl), quartz (Q), biotite (Bt) and muscovite (Mu). Diagrams show a systematic decrease in grain size and standard deviation from weakly deformed granite (LBF stage I) structure to S–C orthogneiss (IWL stage II) structure and banded mylonite (IWL stage III) structure.

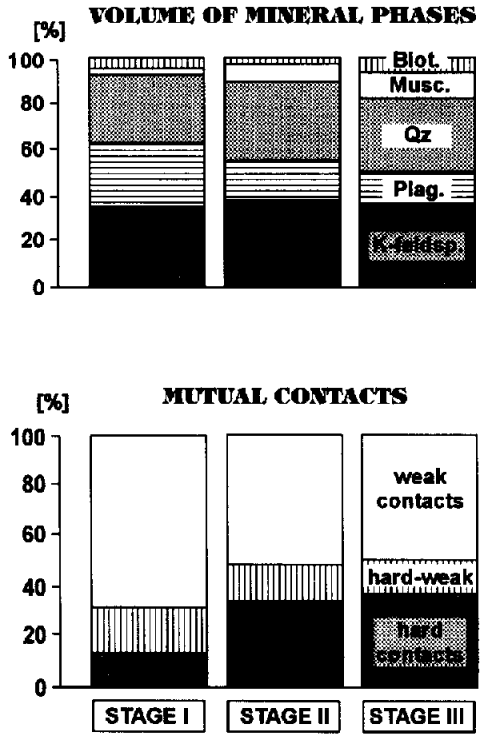


Fig. 6. (a) Modal analyses of granite in three stages of deformation. Note the incipient decrease in plagioclase content and increase in muscovite content with increasing deformation. (b) Mutual contacts of rock-forming minerals in three stages of granite deformation determined using the line-transect method. Hard contacts—contacts between feldspars; weak contacts—contacts between quartz, micas and quartz/mica contacts; hard–weak contacts—weak minerals (quartz, micas) in contact with feldspars. The progressive increase in the number of hard contacts is due to dynamic recrystallization.

nal microstructures are prismatic sub-grain boundaries oblique with respect to the ribbon. Recrystallized micas form isolated bands that commonly separate other mineral aggregates. The amount of new flakes of muscovite increases at the boundaries of recrystallized feldspar grains.

Grain size distribution of individual minerals is very homogeneous (Fig. 5), the grain size of feldspars and micas being almost the same (mean grain size around 50–100 $\mu$m). The modal analysis shows a slight increase in muscovite content in conjunction with a decrease in the plagioclase content (Fig. 6). These facts, together with myrmekite formation, indicate grain-boundary diffusion enhanced by the presence of interstitial fluids. Completely recrystallized feldspars form isolated bands alternating with quartz ribbons and mica layers. Layered structure, composed of bands of recrystallized minerals represents IWL structure with very low viscosity contrast between mineral aggregates.

## BULK ROCK CHEMISTRY AND MINERAL CHEMISTRY

The deformation of granitoids under greenschist facies conditions is accompanied by mineral reactions, e.g. destabilization of plagioclase and of biotite leading to reactional softening in ductile shear zones (Mitra 1978). In contrast, strain-induced mineral reactions and changes in bulk rock chemistry are generally moderate under amphibolite facies conditions (Marquer 1989). The softening mechanism is mainly geometrical (Schmid 1982). In order to estimate the role of syntectonic reactions and, consequently, that of reactional softening on deformation mechanisms and rheology, bulk rock and mineral chemistry of metagranite and orthogneiss have been studied.

The bulk rock chemistry has been studied using X-ray fluorescence (Table 1). The analyses show only slight variations which are in the range of possible initial magmatic fluctuations, even for the most mobile oxides, such as $Na_2O$, CaO, MgO and FeO (Marquer 1989).

Mineral compositions of relict and recrystallized plagioclase, muscovite and biotite were analysed using a

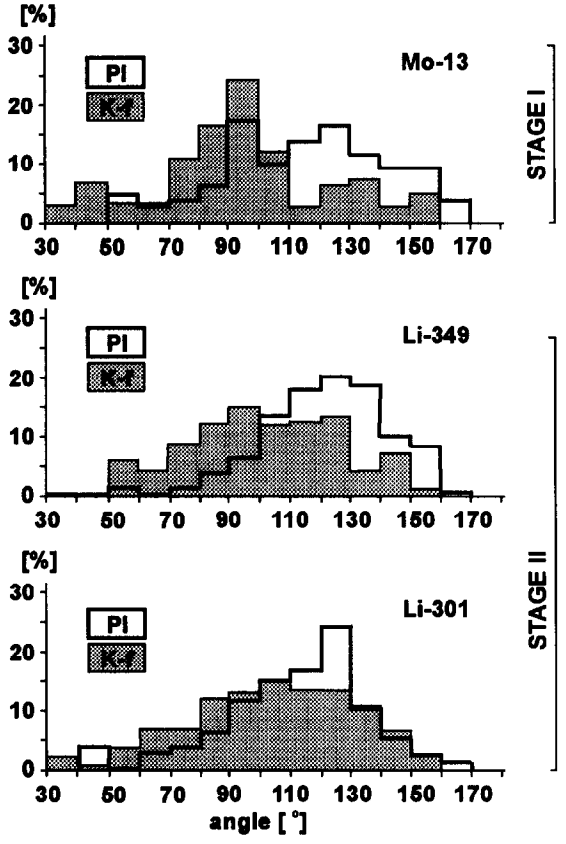


Fig. 7. Histograms showing the distribution of grain boundary angles of recrystallized K-feldspar and plagioclase. K-feldspar new grains are more rectangular than plagioclase. With increasing strain, the degree of annealing increases.

JEOL microprobe of the Czech geological survey. $X_{mg}$ values (0.4–0.45) of large relictual biotite flakes and recrystallized new grains exhibit no systematic changes with increasing strain. The Ti and $Al^{IV}$ content is slightly lower in small recrystallized grains than in parent grains. Recrystallized muscovites show a slight increase of the celadonite component in comparison with large flakes. The Si content of muscovite is 3.3 p.u.f. (per unit formula) in large muscovite crystals of weakly deformed granite and slightly decreases to 3.1 p.u.f. in small new grains in S–C orthogneiss. The chemical composition of recrystallized plagioclase ($An_{20-25}$) does not deviate from those of original clasts.

Using this data, we infer that no significant syntectonic mineral transformations have occurred, except minor neocrystallizations of white mica along plagioclase boundaries and cleavages and local myrmekitization of K-feldspar. Undeformed granite and sheared orthogneiss have comparable chemical compositions, consistent with minor mineral transformations and absence of significant chemical mass transfer.

## ANALYSIS OF GRAIN SHAPE FABRICS

Eighteen samples of deformed orthogneiss were selected for shape analysis. Two sections were cut from each sample parallel to XZ and YZ planes of finite strain. The stretching lineation was considered to represent the X-axis of finite strain and the foliation the XY plane. The lengths of long and short axes and the orientation of the long axis of at least 30 isolated quartz and K-feldspar aggregates were measured on polished XZ and YZ surfaces. The average shape was estimated separately from the quartz and feldspar grains using the Rf/$\phi$ technique (Dunnet 1969). Because of the strong internal anisotropy and viscosity contrast between grains, strain estimates are only semi-quantitative. The results of the shape analysis are displayed on a Flinn (1962) diagram and on the K–R graph of Waterson (1968).

Table 1.

| | Metagranite | | Weakly-deformed granite | S–C Orthogneiss | | |
|---|---|---|---|---|---|---|
| | NV-4 | A-39 | Li-219 | Li-332A | Li-349 | CN-95 |
| $SiO_2$ | 68.62 | 71.12 | 72.26 | 68.31 | 70.30 | 70.74 |
| $TiO_2$ | 0.73 | 0.42 | 0.29 | 0.51 | 0.40 | 0.31 |
| $Al_2O_3$ | 14.81 | 14.33 | 14.46 | 15.51 | 14.86 | 15.02 |
| $Fe_2O_3$ | 0.67 | 0.08 | 1.05 | 1.10 | 0.47 | 0.34 |
| FeO | 2.91 | 2.28 | 1.36 | 2.55 | 2.39 | 2.21 |
| MnO | 0.047 | 0.023 | 0.051 | 0.041 | 0.034 | 0.039 |
| MgO | 1.49 | 0.77 | 0.77 | 1.29 | 1.11 | 0.76 |
| CaO | 1.41 | 1.11 | 0.76 | 1.16 | 1.34 | 1.12 |
| $LiO_2$ | 0.011 | 0.08 | 0.013 | 0.012 | 0.014 | 0.011 |
| $Na_2O$ | 2.71 | 2.64 | 2.71 | 3.02 | 2.55 | 2.75 |
| $K_2O$ | 4.26 | 4.72 | 4.78 | 4.39 | 4.82 | 5.26 |
| $P_2O_5$ | 0.17 | 0.18 | 0.21 | 0.38 | 0.21 | 0.20 |
| $CO_2$ | 0.01 | 0.25 | 0.01 | 0.01 | 0.03 | 0.29 |
| C | 0.03 | 0.03 | 0.01 | 0.01 | 0.01 | 0.01 |
| $H_2O^+$ | 1.40 | 1.18 | 1.71 | 1.98 | 1.49 | 1.36 |
| F | 0.05 | 0.10 | 0.07 | 0.06 | 0.07 | 0.08 |
| S | 0.04 | 0.08 | 0.01 | 0.01 | 0.05 | 0.04 |
| $H_2O^+$ | 0.18 | 0.17 | 0.15 | 0.14 | 0.09 | 0.13 |
| SUM | 99.95 | 99.49 | 100.64 | 100.45 | 100.22 | 100.66 |

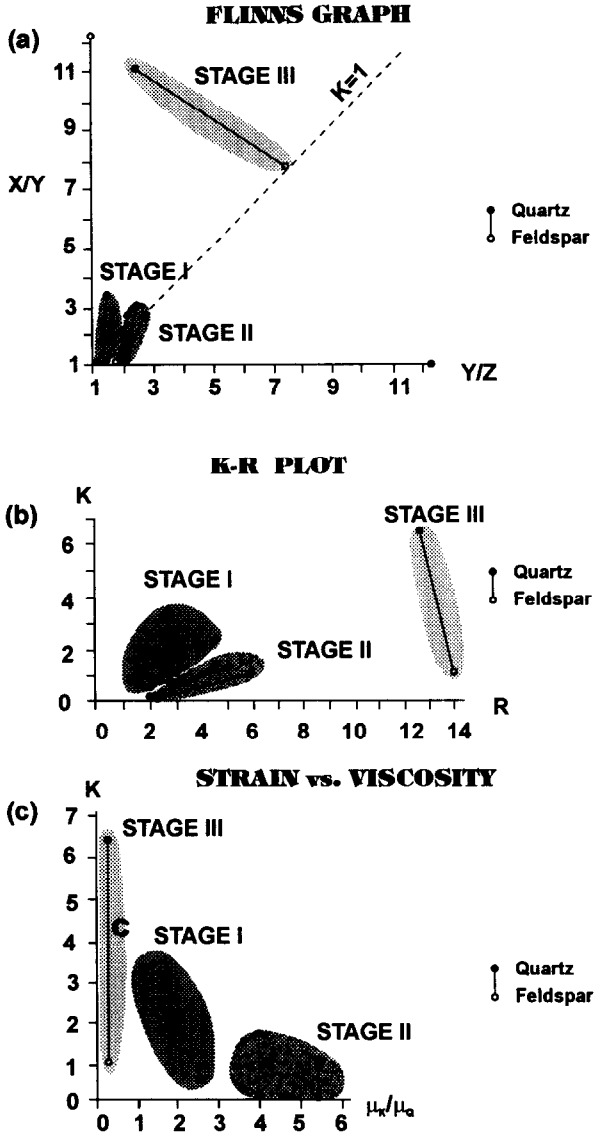


Fig. 8. (a) Flinn's (1962) diagram showing the difference in shape of feldspar (open circles) and quartz aggregates (black circles) with increasing deformation. Quartz and feldspar analyses in one sample are connected by tie-lines. (b) Strain symmetry ($K$) vs strain intensity ($r$) plot (Waterson 1966). Note the difference between feldspar (open circles) and quartz (black circles) aggregates. In stage II quartz and feldspars exhibit similar strain intensities and constrictional shapes. In stage III the oblate and less intense fabrics of feldspars contrasts with intense plane-strain fabrics of quartz. $R$ = X/Y + Y/Z − 1. (c) Plot of strain symmetry ($K$) vs viscosity ratio of feldspars and quartz ($\mu_k/\mu_Q$). Calculation following Gay (1968).

In the weakly deformed granite, quartz is more constrictional in shape than K-feldspar, the latter showing plane strain to constrictional shapes. Quartz exhibits slightly higher strain magnitudes than feldspar (Fig. 8).

In the S–C orthogneiss, K-feldspar aggregates show more oblate symmetry ($k \ll 1$), whereas quartz tends to plot near the $k = 1$ line. Quartz exhibits significantly higher strain intensity than K-feldspar with increasing strain (Fig. 8). The banded mylonite is characterized by shapes of quartz and K-feldspar aggregates which are close to plane strain type, and by very high and similar fabric intensities. Strongly recrystallized feldspar aggregates exhibit locally higher strains than quartz ribbons, indicating that feldspar at this stage could be even weaker than quartz.

In order to study the relationships between strain magnitude and strain symmetry, we have calculated the viscosity ratio between quartz and feldspar. Gay (1968a) defined the viscosity ratio as a measure of viscosity contrast between two pebbles of different viscosity. According to Gay's (1968a, p. 299) equations (3), (4) and (5), the viscosity contrast $\mu_2/\mu_1$ is calculated as a function of ratio of strain ellipticities of more competent and less competent mineral phases. Gay (1968a,b) assumed coherent boundaries among phases throughout the strain history and consequently his approach yields only a minimum estimate of the viscosity contrast (Bilby *et al.* 1975).

The shape analysis in weakly deformed granite yields similar strain intensities and symmetries for quartz and feldspar. Low viscosity contrast (Fig. 8) calculated using Gay's (1968a) equations, however, does not reflect the real difference in viscosity of both phases due to the presence of LBF structure. In such a configuration the hard minerals shield weak pockets (Tharp 1983, Jordan 1987) and consequently the strain intensities of weak and hard phases are not very different.

Increasing deformation leads to the development of mechanical shear instabilities and is accompanied by continuous increase in difference of strain magnitude and fabric symmetry between quartz and feldspar (Fig. 8). This transition to IWL structure allows the use of measured shape differences for viscosity contrast calculations. The progressive deformation was increasingly accommodated by quartz layers, resulting in an increase in the strain intensity of quartz aggregates. In contrast, the feldspar aggregates composed of relic cores and recrystallized tails reveal only a change to more oblate shapes and no increase in fabric magnitude.

The banded mylonite exhibits similar shapes of quartz and feldspar aggregates and also similar fabric intensities. The abrupt increase of feldspar deformability is associated with its total recrystallization leading to a considerable decrease of the viscosity ratio between quartz and feldspar. All these progressive changes in shape fabric symmetry and magnitude are clearly associated with microstructural changes in individual phases and overall grain refinement influencing real viscosities of composite material.

## CRYSTALLOGRAPHIC PREFERRED ORIENTATION

### *Evolution of quartz c-axis patterns*

Orientations of quartz c-axes have been obtained from thin-sections cut parallel to XZ and YZ planes of finite strain using the universal stage. The grain sizes of recrystallized quartz grains have been measured using the line-transect method.

Quartz in stage I metagranite occurs as large blebs with dynamically recrystallized boundaries and intense

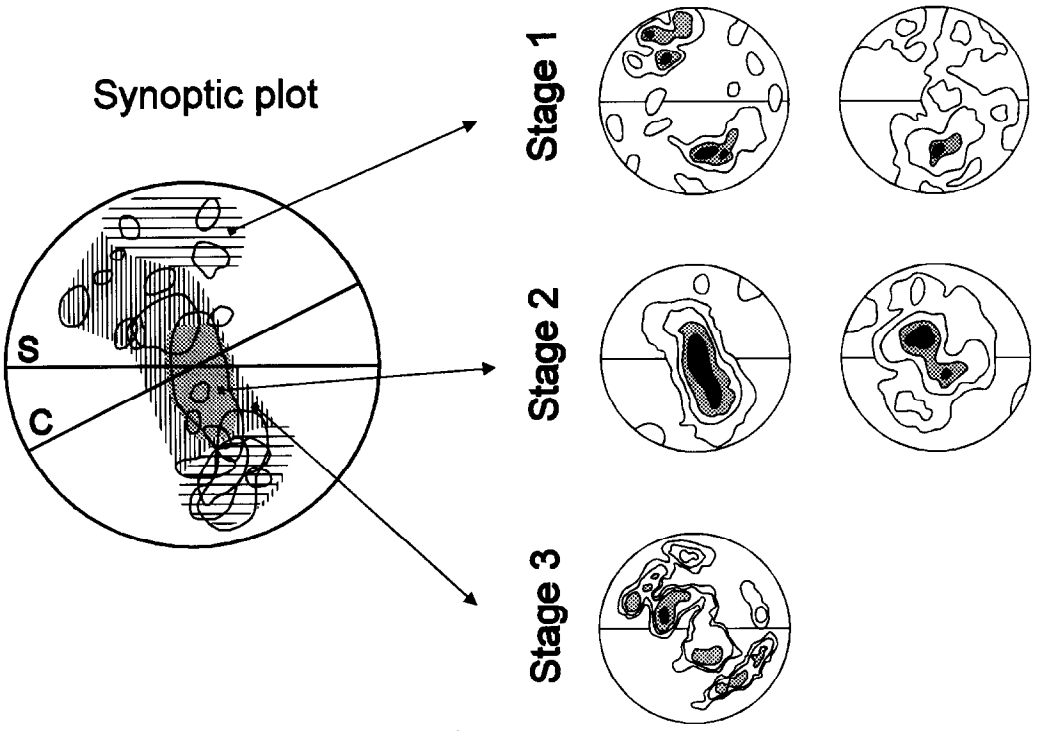


Fig. 9. Quartz c-axis patterns for three stages of granite deformation. Lower hemisphere equal-area projections. Foliation is represented by horizontal line, lineation is horizontal in E–W direction. Contours in multiples of uniform distribution: stage I, 1, 1.5, 2, 2.5, × u.d., 74 measurements; stage II, 1, 2.5, 3.5, 4.5 × u.d., 200 measurements; stage III, 1, 2.5, 3.5, 5 × u.d., 200 measurements. The synoptic plot of all maxima of c-axis > 4 × u.d. showing fabric evolution.

prismatic subgrains in the core. The c-axis fabric (Fig. 9) is weak with a faint tendency to form an unequally developed girdle distribution (type I in Lister 1977). As this c-axis fabric is probably influenced by the initial orientation of the large host grains (Van Roermund *et al.* 1979), an unequivocal interpretation is not possible.

C-axis fabrics in weakly deformed granite show type I distribution of Lister (1977) with one dominant and one subordinate girdle (Fig. 9). The dominant girdle is oblique to the structural framework defined by the finite strain axes. The geometrical relationship between prismatic sub-boundaries and c-axis orientation (Fig. 9) suggests that dominant basal ⟨a⟩ slip was active during deformation (Bouchez 1977, Vauchez 1980). This is supported by the position of maxima in crossed-girdles (Fig. 9) near the periphery of the diagram.

In strongly deformed S–C granites, the grain size reduction of quartz and development of grain shape oblique fabric with respect to the ribbon boundary (Lister & Snoke 1984) is connected with different quartz c-axis patterns exhibiting an oblique girdle with strong maximum near the Y-axis of finite strain. The uniform grain size, larger elongate grains, smaller sub-equant grains, and the very homogeneous c-axis orientation indicate a combination of predominantly migration, recrystallization and prismatic ⟨a⟩ glide in quartz (Schmid & Casey 1986).

Quartz C-axis patterns within ribbons of banded mylonite exhibit a typical single girdle oblique to the foliation and the lineation. The principal maxima are situated between the periphery of the diagram and its centre indicating predominant activity of combined basal ⟨a⟩, basal ⟨a+c⟩ and prism ⟨a⟩ slip (Schmid & Casey 1986).

A synoptic plot of all the quartz c-axis maxima shows a great girdle oblique to the structural framework defined by the finite strain axes X, Y, Z (Fig. 9). The girdle has a constant width of 20° and is orthogonal to the shear direction defined by foliation and ubiquitous C planes. The stable position of the girdle indicates little change in the kinematics regime during shear (Lister & Williams 1979).

Observed switch of slip system in quartz from basal ⟨a⟩ in LBF structure, to prism ⟨a⟩ in orthogneiss structure and finally to basal ⟨a⟩ and rhomb ⟨a+c⟩ in banded mylonite is related to significant changes in quartz grain size and increase of strain intensity. Observed changes in quartz c-axis patterns and switches in activities of slip systems may therefore be attributed to variations of flow stress and strain rate rather than to changing temperature during deformation. We suggest that similar relationships between slip system changes and stress variations could be valid for feldspars.

### *Crystallographic preferred orientation of K-feldspar and plagioclase*

Orientations of crystallographic axes of host and new grains of plagioclase and K-feldspar have been determined using a U-stage. Both host- and recrystallized K-feldspar grains in S–C granite exhibit strong preferred crystallographic orientations with $\beta$ subparallel to L, $\gamma$ perpendicular to S and $\alpha$ perpendicular to L and parallel to S. Differences in orientation between new grains and

the host are in the range 10–60° with a maximum around 10–20°, indicating that the orientation of the megacryst determines that of the new grains (Debat *et al.* 1978, Vidal *et al.* 1979).

Optical crystallographic preferred orientation in S–C orthogneiss is less pronounced than that of stage I metagranite. The mean value of new grain misorientation with respect to relics of the host is about 40°, indicating loss of crystallographic control of the host on new grains.

In S–C orthogneiss, plagioclase shows a strong preferred orientation, with $\beta$ axes forming two maxima parallel to either the X- or Y-axis of finite strain (Fig. 10). The $\alpha$ direction forms crossed girdles, with the most pronounced maximum parallel to the Y-axis of finite strain, and $\gamma$ showing a maximum parallel to the Z-axis. The host control of large relict grains on crystallographic preferred orientation of neoblasts is much weaker for plagioclase than for K-feldspar.

In banded mylonites the optical axes of recrystallized K-feldspars show a strong crystallographic fabric, with $\alpha$ and $\gamma$ axes distributed in broad perpendicular maxima around the periphery of the diagram, oblique to the Z-axis of finite strain (Fig. 10). The $\beta$-axes are symmetrically distributed around the Y strain axis.

*Significance of feldspar microfabrics*

Very strong crystallographic preferred orientation of K-feldspar relictual grains and of neoblasts in weakly deformed granite show that dislocation glide is the dominant deformation mechanism associated with dynamic recrystallization. The fabric pattern may be interpreted as the result of glide on (010) planes in the ⟨001⟩ direction. The important crystallographic control of orientation of new grains on the host clasts indicates rotation recrystallization. The active slip system in K-feldspar of banded mylonite is (010)⟨100⟩. Slip on this system has been obtained experimentally at a temperature of around 700° and a strain rate of $10^{-6}\,s^{-1}$ (Tullis & Yund 1977). (010)⟨001⟩ slip was also reported from high-grade naturally deformed rocks (Tullis 1983).

The geometrical relationships between the optical indicatrix and the crystallographic axes in the plagioclase varies according to the anorthite content (Ji & Mainprice 1988). For oligoclase the optical directions $\alpha$ and $\beta$ are almost parallel to (100) and (001), respectively, and $\gamma$ is perpendicular to (010).

Fabrics of plagioclase relicts and neoblasts are similar to those found by Ji & Mainprice (1988) and Olsen & Kohlstedt (1985). Following these authors, we suggest glide on (010) plane, dominantly in (001) or (100) directions. This type of slip system is generally reported for high-grade (amphibolite facies or granulite facies) tectonites (Tullis 1983).

## DISCUSSION AND CONCLUSIONS

Deformation of the Erzgebirge pre-Variscan granitoids is strongly partitioned at the map scale and leads to the occurrence of three types of deformed rock: (1) slightly deformed granite, (2) S–C granite representing the largest volumes of rock, and (3) narrow zones of banded mylonite.

Several observations document that, in the initial stage of deformation, the granite structure may be compared with LBF microstructure (Tharp 1983, Jordan 1988, Handy 1990):

(1) There are only slight differences in deformation intensity of hard and weak minerals. This implies that the deformation of the weaker quartz is limited by that of feldspar network.

(2) The shapes of hard and weak phases are similar—both in the field of apparent constriction. At this stage the shapes of mineral aggregates probably reflect the strain symmetry.

The deformation of feldspars at this stage occurs probably in the transient region between brittle and plastic behavior as indicated by fracturing and the onset of dynamic recrystallization along microshears. Dynamic recrystallization of plagioclase is much more important than in K-feldspar. At the same deformation stage, deformation of large recrystallized quartz grains is characterized by weak crystallographic preferred orientation, with activity of basal ⟨a⟩ glide and fast boundary migration.

These microstructures are consistent with the presence of LBF structure in which the strain is uniformly distributed and stress is concentrated in the strong framework (Handy 1994a). Skeleton-forming K-feldspars are deformed inhomogeneously and recrystallized microshears accommodate most of the imposed strain within the framework, while plagioclase is deformed more homogeneously. In contrast, large recrystallized quartz grains indicate lower stress in the weaker phase. Weak preferred orientation of c-axes may be due to low bulk strain in homogeneously deformed quartz aggregates.

The LBF structure is considered to be highly unstable during rock deformation (Handy 1990, 1994a). Even small strains lead to breakdown of the rigid skeleton and to the development of thin, interconnected weak layers. The rheology of granitoids is influenced by the presence of weak quartz and stronger K-feldspar and plagioclase which, however, exhibit different strengths. The activation energy of dynamic recrystallization and dislocation glide is lower for plagioclase than for K-feldspar, but is still much higher than for quartz under middle to high homologous temperatures (Gapais 1989, Fitz Gerald & Stunitz 1993). In fact, the mechanism of deformation of rigid K-feldspar is mostly fracturing, while the plastic behaviour of plagioclase accommodates surface incompatibilities and may prolong the stability field of the LBF structure. The LBF structure can help to answer questions about the role of strain energy as a direct cause of myrmekite growth at early stages of deformation. Simpson & Wintsch (1989) argued that myrmekite formation is localised at high-pressure sides of K-feldspar clasts (long faces of the clasts) due to the role of stress in myrmekite-forming reactions. In con-

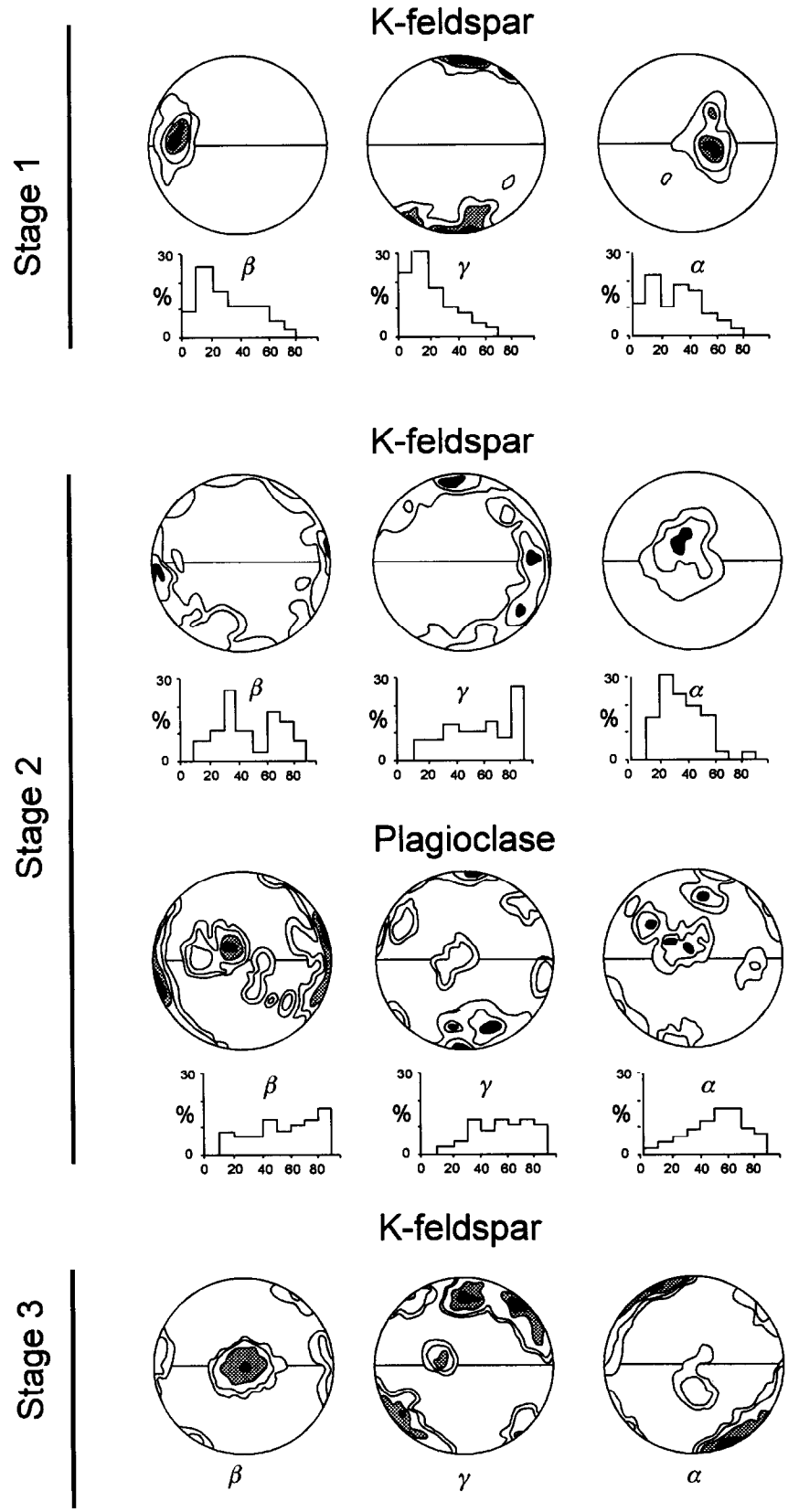


Fig. 10. Preferred orientations of optical directions $\alpha$, $\beta$ and $\gamma$ of recrystallized K-feldspar and plagioclase grains. Histograms show the angular difference between the host grain and recrystallized new grains. Note decrease in fabric intensity, loss of host control on the orientation of new grains during stage II and the change of slip system during stage III.

trast Vernon (1991) argued that myrmekite lobes do not grow in high-strain environments. The stress in the LBF structure is concentrated at mutual contacts of hard minerals rather than along their long faces. Thus, the replacement of K-feldspar by myrmekites occurs preferentially in areas relatively protected from deformation rather than in high stress sites. The migration of quartz boundaries in the interstitial sites of the framework also supports the importance of self-diffusion processes in stress-protected zones.

Deformation is accompanied by overall grain-size reduction associated with an increase in the volume fraction of the recrystallized weak phase. These factors contribute to the breakdown of the feldspar skeleton and to the switch from LBF structure to IWL structure with increasing deformation. At this stage of granite deformation, typical S–C orthogneiss with oval feldspar augens develop. The orthogneiss structure is characterized by the following features:

(1) The amount of strain affecting the weak quartz is significantly higher than that of feldspars.

(2) Feldspar aggregates formed by relict clasts and recrystallized tails exhibit more oblate forms than quartz. The later forms ribbons of plane-strain shapes with grain-shape oblique internal foliation (Knipe & Law 1987). Recrystallized quartz exhibits strong grain size variations and evidence for dominant prism ⟨a⟩ slip.

(3) Completely recrystallized feldspar grains around relictual clasts reveal glide on (010) planes in ⟨001⟩ direction and better annealed foam textures in the IWL stage compared to the LBF stage.

This strain partitioning between quartz and feldspar layers resembles that recognized in metapelites (Bell 1985), where non-coaxial deformation is concentrated into mica-rich layers and bulk shortening in quartz-rich ones. In this context it is possible to compare the oblate zones of annealing in pressure shadows around feldspars with the sites of nucleation and porphyroblast growth in metapelites. Regions exhibiting annealing textures develop in pressure shadows around rigid clasts where stresses and strain rates are small. Deformation partitioning into zones of progressive non-coaxial deformation and progressive shortening, controlling zones of recovery and dynamic recrystallisation in feldspar mylonite, was in a similar manner reported by Bell & Johnson (1989) in feldspar mylonites.

Most of the deformation at this stage is concentrated in quartz layers which, as indicated, are supported by their intense plastic deformation, variations in grain size and strong preferred orientation of c-axes. A switch in the dominant slip system in quartz from basal ⟨a⟩ to prism ⟨a⟩ is accompanied by grain size reduction down to several tens of $\mu$m (the size of new quartz grains and other constitutive minerals is similar). This is in agreement with observations in quartzites and quartz–feldspar mylonites where prism glide is activated at higher resolved shear stress and higher strain rates than basal and rhomb glide (Schmid & Casey 1986, Handy 1990).

The concentration of deformation into the weak quartz layers is the main characteristic for the IWL structure with a low proportion of weak phase and/or of high viscous strength contrast between strong and weak phases (Handy 1994a,b). We suppose that the viscosity contrast between the weakest quartz and plagioclase is much higher than that between K-feldspar and plagioclase. Consequently, when quartz becomes interconnected and rheologically active, the behaviour of rock approaches that of a two-phase material, i.e. weak quartz and stronger feldspars. Hence, in the structural stability diagram of Handy (1994a) the calculated viscosity ratio between feldspar and quartz is plotted against the volume of quartz representing the amount of weak phase.

The final stage of granite deformation is represented by the development of banded mylonitic structure in narrow zones. This structure is characterized by the following features:

(1) The deformation intensity and degree of prolateness of feldspar aggregates is higher than that of quartz ribbons. At this stage all minerals are completely recrystallized and form approximately monomineral aggregates.

(2) Quartz grain size increases with respect to the orthogneiss stage. Quartz shows also a switch from prism ⟨a⟩ typical for orthogneiss (stage II) to dominant basal ⟨a⟩ and rhomb ⟨a+c⟩ slip. The active slip system in K-feldspar switches from (010) ⟨001⟩ in orthogneiss to (010)⟨100⟩ in banded mylonite.

The structural stability diagram (Fig. 11) for the quartz–feldspar rocks of Handy (1994a) shows the microstructural and rheological evolution of Erzgebirge granitoids. Analyses of mineral volumes (Fig. 6) as well as chemical analyses (Table 1) of deformed granitoids show relatively stable rock composition during deformation. Therefore, we have plotted constant quartz volume against corresponding measured viscosity contrasts for both the orthogneiss stage and banded mylonite.

The rheological evolution of the rock shows breakdown of LBF structures at relatively small strains and a switch to IWL structure with high viscosity contrast between weak and strong phases. This type of structure prevails at intermediate strain intensities and switches to IWL structure with low viscosity contrast between strong and weak phase at very high strains. This type of structural evolution is consistent with results of experimental work by Jordan (1987). Grain size/flow stress changes of recrystallized quartz are associated with a switch of slip system in quartz from basal ⟨a⟩ in LBF structure, to prism ⟨a⟩ in orthogneiss structure and finally to basal ⟨a⟩ and rhomb ⟨a+c⟩ in banded mylonite. High stress intensity in weak quartz layers of S–C orthogneiss is related with high stress concentration due to large feldspar clast size and small spacing factor (Handy 1990). In banded mylonite the stress concentration decreases significantly due to small clast (recrystallized feldspar bands) sizes and large spacings between feldspar layers.

The transition from granite to banded mylonite is also associated with a significant decrease of bulk rock strength due to foliation weakening predicted by Jordan (1988) and Handy (1990). Finally, the fully recrystallized feldspars show the same rheological activity as quartz in banded mylonite, which probably represents a steady state microstructure.

*Acknowledgements*—Many thanks to Jean Pierre Burg, Mark Handy and Holger Stunitz for significant improvements of the first draft of the manuscript and for fruitful discussions. We are grateful to an anonymous reviewer and Paul Bons for careful review of this paper. We

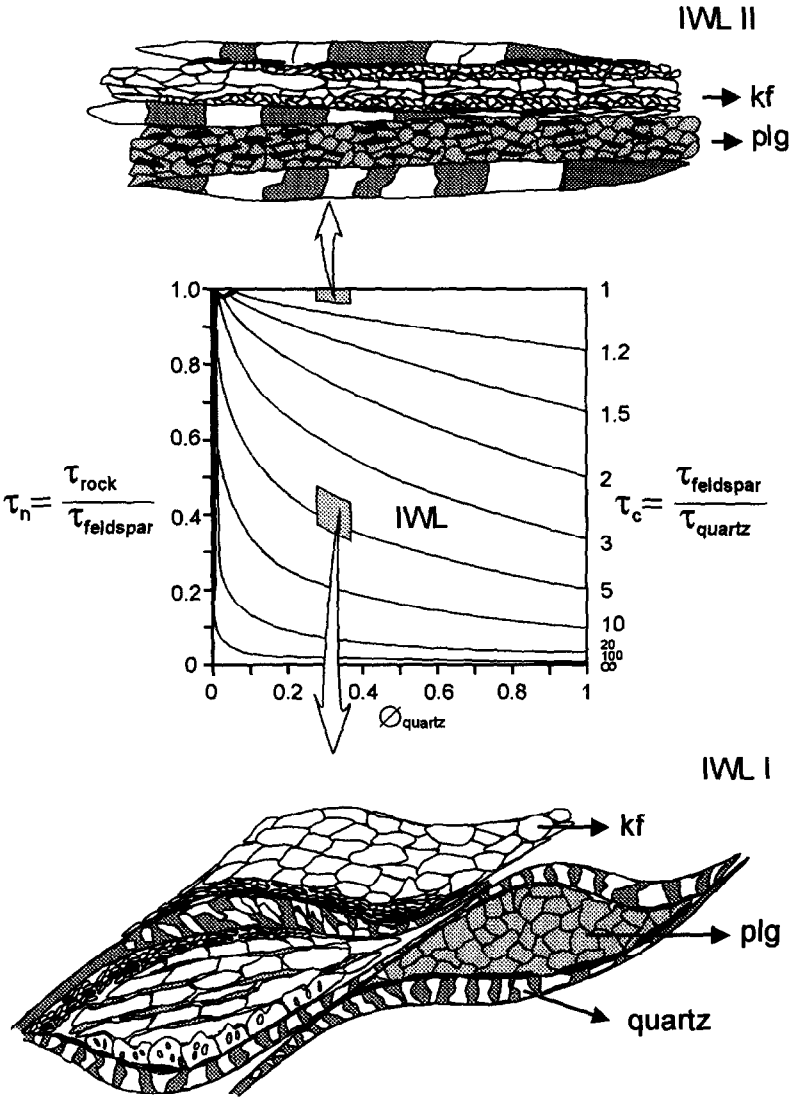


Fig. 11. Structural stability diagram for deformed Erzgebirge granitoids. Rock strength on the left/hand axis is normalized to the viscosity of feldspar. Viscosity ratio of K-feldspar and quartz is plotted on the right/hand axis. Viscosity ratios of IWL structures are calculated using Gay's (1968) equations. The upper and lower insets show the characteristic microstructures for S–C orthogneiss, IWL structure and banded mylonite structure.

thank Vladimir Tolar for drawing the figures. This work was supported by a grant from the Czech National Foundation of the Czech Republic, No. 205-93-0709.

## REFERENCES

Bell, T. H. 1985. Deformation partitioning and porphyroblast rotation in metamorphic rocks: a radical reinterpretation. *J. Metamorphic Geol.* **3**, 109–118.

Bell, T. H. & Johnson, S. E. 1989. The role of deformation partitioning in the deformation and recrystallization of plagioclase and K-feldspar in the Woodroffe thrust mylonite zone, central Australia. *J. Metamorphic Geol.* **7**, 151–168.

Berthé, D., Choukroune, P. & Jegouzo, P. 1979. Orthogneiss, mylonite and non-coaxial deformation of granites: the example of south Armorican Shear zone. *J. Struct. Geol.* **2**, 127–133.

Bilby, B. A., Eshelby, J. D. & Kundu, A. K. 1975. The change of shape of a viscous ellipsoidal region embedded in a slowly deforming matrix having different viscosity. *Tectonophysics* **28**, 265–274.

Bossiére, G. & Vauchez, A. 1978. Déformation naturelle par cisaillement ductile d'un granite de Grande Kabylie (Algerie). *Tectonophysics* **51**, 57–81.

Bouchez, J. L. 1977. Plastic deformation of quartzites at low temperatures in an area of natural strain gradient. *Tectonophysics* **39**, 25–50.

Burg, J. P. & Laurent, Ph. 1978. Strain analysis of a shear zone in a granodiorite. *Tectonophysics* **47**, 15–42.

Christie, J. M., Ord, A & Koch, P. S. 1980. Relationship between recrystallized grain-size and flow-stress in experimentally deformed quartzite. *Trans. Am. Geophys. Un.* **61**, 377.

Debat, P., Soula, J. C., Kubin, L. & Vidal, J. L. 1978. Optical studies of natural deformation, microstructures in feldspars (gneiss and pegmatites from Occitania, southern France). *Lithos* **11**, 133–145.

Dunnet, D. 1969. A technique of finite strain analysis using elliptical particles. *Tectonophysics* **7**, 117–136.

Fitz Gerald, J. D. & Stunitz, H. 1993. Deformation of granitoids at low metamorphic grade. I: Reactions and grain size reduction. *Tectonophysics* **221**, 269–297.

Flinn, D. 1962. On folding during three dimensional progressive deformation. *Q. Jl Geol. Soc. Lond.* **118**, 385–433.

Gapais, D. 1989a. Les orthogneiss: Structures, mécanismes de déformation et analyse cinématique. (Exemple du granite de Flamanville), *Mémoires et Documents du Centre Armoricain d'Etude Structurale des Socles*, 366 pp.

Gapais, D. 1989b. Shear structures within deformed granites: mechanical and thermal indicators. *Geology* **17**, 1144–1147.

Gay, N. C. 1968a. Pure shear and simple shear deformation of inhomogeneous viscous fluids, part II: the deformation of the total finite strain in a rock from objects such as deformed pebbles. *Tectonophysics* **5**, 211–234.

Gay, N. C. 1968b. Pure shear and simple shear deformation of inhomogeneous viscous fluids, part 2: the deformation of the total

finite strain in a rock from objects such as deformed pebbles. *Tectonophysics* **5**, 295–302.
Handy, M. R. 1990. The solid state flow of polymineralic rocks. *J. geophys. Res.* **95**, 8647–8661.
Handy, M. R. 1994a. Flow laws for rocks containing two nonlinear viscous phases: a phenomenological approach. *J. Struct. Geol.* **3**, 287–301.
Handy, M. R. 1994b. The energetics of steady state heterogeneous shear in mylonitic rocks. *Mat. Sci. Eng.* **A175**, 261–272.
Hanmer, S. K. 1982. Microstructure and geochemistry of plagioclase and microcline in naturally deformed granite. *J. Struct. Geol.* **4**, 197–215.
Jessel, M. 1986. Grain boundary migration microstructures in a naturally deformed quartzite. *J. Struct. Geol.* **9**, 1007–1014.
Ji, S. & Mainprice, D. 1988. Natural deformation fabrics of plagioclase: Implications for slip systems and seismic anisotropy. *Tectonophysics* **147**, 145–163.
Jordan, P. G. 1987. The deformational behaviour of bimineralic limestone-halite aggregates. *Tectonophysics* **135**, 185–197.
Jordan, P. G. 1988. The rheology of polymineralic rocks—An approach. *Geol. Rdsch.* **77**, 285–294.
Knipe, R. J. 1989. Deformation mechanisms—recognition from natural tectonites. *J. Struct. Geol.* **11**, 127–146.
Knipe, R. J. & Wintsch, R. P. 1985. Heterogeneous deformation, foliation development and metamorphic processes in a polyphase mylonite. In *Metamorphic reactions, kinetics, textures and deformation* (edited by A. B. Thompson & D. C. Rubie), Springer Verlag, Berlin, Germany.
Knipe, R. J. & Law, R. D. 1987. The influence of crystallographic orientation and grain boundary migration on microstructural and textural evolution in an S–C mylonite. *Tectonophysics* **135**, 155–169.
Kröner, A., Willner, A. P., Hegner, E., Frischbutter, A., Hofman, J. & Bergner, R. in press. Latest Precambrian (Cadomian) zircon ages: Nd isotopic systematics and PT evolution of granitoid orthogneiss of the Erzgebirge, Saxony and Czech Republic. *Geol. Rdsch.*
Lister, G. S. 1977. Crossed-girdle c-axis fabrics in quartzites plastically deformed by plane strain and progressive simple shear. *Tectonophysics* **39**, 51–54.
Lister, G. S. & Williams, P. F. 1979. Fabric development in shear zones: Theoretical controls and observed phenomena. *J. Struct. Geol.* **1**, 283–297.
Lister, G. S. & Snoke, A. W. 1984. S–C mylonites. *J. Struct. Geol.* **6**, 617–638.
Marquer, D. 1989. Transfert de matiere et deformation des granitoides, aspect methodologiques. *Schweiz. Mineral. Petrogr. Mitt.* **69**, 15–35.
Mitra, G. 1978. Ductile deformation zones and mylonites: The mechanical processes involved in the deformation of crystalline basement rocks. *Am. J. Sci.* **278**, 1057–1084.
Mlcoch, B. & Schulmann, K. 1991. Superposition of Variscan ductile shear deformation on pre-Variscan mantled gneiss structure (Catherine dome, Erzgebirge, Bohemian Massif). *Geol. Rdsch.* **81**, 501–513.
Poirier, J. P. & Guillope, M. 1978. Deformation induced recrystallization of minerals. *Bull. Soc. fr. Minér. Cristallogr.* **102**, 67–74.
Scheumann, K. H. 1932. Uber die petrographische Ableitung des roten Erzgebirg gneisses. *Tschermaks Mineral. Petr. Mitt.* **42**, 414–454.
Schmid, S. M. 1982. Microfabric studies as indicators of deformation mechanisms and flow laws operative in mountain building. In *Mountain building processes* (edited by K. Hsu).
Schmid, S. M. & Casey, M. 1986. Complete fabric analysis of some commonly observed quartz c-axis patterns. In *Mineral and rock deformation: Laboratory studies. Geophys. Monogr. Ser.* **36**. (edited by B. E. Hobbs & H. C. Heard) AGU, Washington, D.C., USA, pp. 236–286.
Simpson, C. 1985. Deformation of granitic rocks across the brittle-ductile transition. *J. Struct. Geol.* **7**, 503–511.
Simpson, C. & Wintsch, R. P. 1989. Evidence for deformation induced K-feldspar replacement by myrmekite. *J. Metamorphic Geol.* **7**, 261–275.
Tharp, T. M. 1983. Analogies between high temperature deformation of polyphase rocks and the mechanical behaviour of porous powder metal. *Tectonophysics* **96**, 1–11.
Tullis, I. & Yund, R. A. 1977. Experimental deformation of dry Westerly granite. *J. Geophys. Res.* **82**, 5705–5718.
Tullis, I. 1983. Deformation of feldspars. In *Feldspar mineralogy*, 2nd edn. (edited by P. H. Ribbe), *Min. Soc. Am. Rev. Mineralogy* **2**, 297–323.
Van Roermund, V. H., Lister, G. S. & Williams, P. F. 1979. Progressive development of quartz fabrics in a shear zone from Monte Mucrone, Sesia-Lanzo zone, Italian Alps. *J. Struct. Geol.* **1**, 43–52.
Vauchez, A. 1980. Ribbon structure and deformation mechanisms of quartz in mylonitised granite of Great Kabylia (Algeria). *Tectonophysics* **67**, 1–12.
Vauchez, A. 1987. The development of discrete shear zones in granite: Stress, strain and changes in deformation mechanisms. *Tectonophysics* **133**, 137–156.
Vernon, R. H. 1991. Questions about myrmekite in deformed rocks. *J. Struct. Geol.* **133**, 979–985.
Vidal, J. L., Kubin, L., Debat, P. & Soula, J. C. 1979. Deformation and dynamic recrystallization of K-feldspar augen in orthogneiss from Montagne Noir, Occitania, Southern France. *Lithos* **13**, 247–255.
White, S. H. 1975a. The effects of strain on the microstructures, fabrics and deformation mechanism in quartzites. *Phil. Trans. R. Soc. Lond.* **A283**, 69–86.
White, S. H. 1975b. Tectonic deformation and recrystallization of oligoclase. *Contr. Miner. Petrol.* 50, 287–304.
White, S. H., Burrows, S. E., Carreras, J., Shaw, N. D. & Humphreys, F. J. 1980. On mylonites in ductile shear zones. *J. Struct. Geol.* **2**, 175–187.
Waterson, J. 1968. Homogeneous deformation of the gneisses of Vesterland, southwest Greenland. *Bull. Gronl. Geol. Unders.* **175**, 1–78.